JOURNAL OF COMPUTATIONAL PHYSICS 111, 390–398 (1994)

Rapid Pulse Responses for Scattering Problems*

GREGORY A. KRIEGSMANN AND JONATHAN H. C. LUKE

Department of Mathematics, Center for Applied Mathematics and Statistics, New Jersey Institute of Technology, University Heights, Newark, New Jersey 07102

Received January 6, 1993; revised July 6, 1993

Numerical computation of the field scattered from a body in two dimensions due to an incident plane pressure pulse is considered. In particular, we examine the process of inferring the scattered field due to one incident pulse given the scattered field due to another incident pulse. The objective is to develop an indirect method that avoids the potentially expensive direct solution of the problem. Our approach is based on a formula expressing the scattered field as a convolution of a kernel with the incident pulse profile. The most straightforward generalization of this formula to the discrete version of the scatterer problem used in numerical computations does not allow the kernel to be inferred from a single numerical experiment—a difficulty we call the *multi-source problem*. Preprocessing the incident pulses using simple interpolation formulas overcomes the multi-source problem giving an exact algorithm for computing the kernel. Selection of a sharp incident pulse (the Kronecker pulse) for the primary numerical experiment assures stability of this algorithm and permits extremely accurate prediction of the scattered fields for secondary incident pulses.

I. INTRODUCTION

We are concerned here with the scattering of a plane pressure pulse $u(x, y, t) = U(x + t)$ from an impenetrable target S. The determination of the scattered wave $v(x, y, t)$ usually requires a numerical method, such as finite differences or time-dependent integral-equation techniques [1, 2]. The computational burden of such a method depends upon the complexity of the target geometry and upon the high frequency content of U. If this burden is significant, then the determination of a second response $\tilde{v}$ due to another incident pulse $\tilde{u}(x, y, t) = \tilde{U}(x + t)$ by the same method may be prohibitive. We present here a method of using the results from the first simulation to indirectly and more efficiently determine those of the second.

The notion of determining the response of a linear system, for a given input, from its response to a delta function input forms the backbone of systems analysis. In the context of scattering theory the analog is contained in the relationship

$$\tilde{v}(x, y, t) = \int_{-\infty}^{t} K(x, y, t-\tau)\, \tilde{u}(x, y, \tau)\, d\tau \qquad (1.1)$$

which expresses the new scattered field $\tilde{v}$ as the convolution of its associated incident field $\tilde{u}$ and the target response, K, to an incident plane delta function. This formula is solely a consequence of the linearity of the governing wave equation and boundary conditions, and Fourier analysis. It is, however, of limited value because it is difficult to numerically model an incident delta function and to compute its response.

Another equivalent approach follows along the following lines of reasoning. When a response is computed for a given incident pulse, post processing by Fourier transforms will yield the response of the target for a plane wave of a given frequency. These responses can be weighted and resummed to produce the scattered field for another incident pulse. Applying standard transform techniques this procedure yields the generalization of (1.1)

$$\tilde{v}(x, y, t) = \int_{-\infty}^{t} g(t-\tau)\, v(x, y, \tau)\, d\tau \qquad (1.2a)$$

$$g(\tau) = \frac{1}{2\pi} \int_{-\infty}^{\infty} \frac{\tilde{A}(k)}{A(k)}\, e^{ik\tau}\, dk \qquad (1.2b)$$

where A and $\tilde{A}$ are the Fourier transforms of the incident pulses u and $\tilde{u}$, respectively. The applicability of this method profoundly depends upon the relationship between the spectral densities of both incident pulses and may not be robust depending on their behavior at infinity.

In this paper we shall present a new method which is based upon a numerical analog of (1.1). Pivotal in the method is our ability to obtain an approximation of the kernel K which, as was mentioned above, is the response to an incident delta plane wave. This is achieved by running one

* This work was supported by the Air Force Office of Scientific Research under Grant No. AFOSR 91-0252 and by the Office of Naval Research under Grant N0014-92-J-1261.

0021-9991/94 $6.00

numerical experiment with an incident pulse given by a linear approximation to a Kronecker delta function, i.e., a function that is unity at one grid point, zero elsewhere, and linearly defined in between. Although this pulse is at best a poor approximation to a delta function, the algorithm we present shows that its response explicitly yields a numerical approximation to K. This is then used in our discrete analog of (1.1) to obtain numerical approximations to the scattered field for any incident pulse. In particular when the incident plane wave is a stepped time-harmonic plane wave, our method yields an explicit expression for the scattered field, which for large times goes to the time-harmonic response. Thus, time-harmonic responses can be deduced in a much more efficient manner than using FDTD codes. The latter are essentially explicit iteration schemes which typically begin with quiescent initial conditions and converge to the time-harmonic response caused by an incident stepped plane wave [3–5]. We note, however, that our method is faithful to the underlying finite-difference scheme. That is, the errors present in the direct finite-difference simulation of the scattering problem for a given incident pulse are exactly reproduced by our method.

We shall now briefly outline the remainder of the paper. In Section 2 we formulate the prototypical scattering problem in which an incident plane pulse impinges upon a sound-soft target. We then analyze a general class of numerical methods and derive, by first preconditioning the incident pulse, a formula which is the discrete analog of the continuous convolution result (1.1). A simple algorithm is then presented which gives a numerical approximation to $\tilde{v}$ in terms of v and $\tilde{U}$. In Section 3 we test out our method on the scattering of waves from a sound-soft circular cylinder.

II. NUMERICAL CONSIDERATIONS

In this section we consider numerical implementation of a secondary pulse prediction procedure. In the context of a large class of numerical methods for computing the primary scattered wave, we derive an exact procedure for computing secondary scattered waves without reuse of the numerical method. An explicit representation formula characterizing the class of numerical methods is the foundation of our procedure. The most interesting aspect of the derivation is an unexpected difficulty (here called the *multi-source problem*) that arises from discretization. We overcome this problem with a modification of the incident pulses that assures they share certain properties. That is, the exact prediction of the secondary scattered wave requires particular relationships between the pulses. Fortunately, for many pairs of incident pulses and many numerical methods, the modification of the pulses needed to produce the required relationships is negligible compared to the errors inherent in the numerical method.

Problem Formulation

To illustrate our method we shall study a simple two-dimensional acoustic scattering problem in which a plane pulse $u = U(x + t)$ insonifies a sound-soft target S and scatters from it. We assume that the pulse first strikes the target at $t = 0$; i.e., $U(x + t) = 0$ when $t < 0$ and $(x, y) \in S$. Then letting D denote the exterior of the target, the scattered wave $v(x, y, t)$ is the solution of the exterior initial-boundary value problem:

$$v_{tt} - v_{xx} - v_{yy} = 0, \qquad (x, y) \in D, \qquad t > 0 \tag{2.1a}$$

$$v(x, y, 0) = 0, \qquad (x, y) \in D \tag{2.1b}$$

$$v_t(x, y, 0) = 0, \qquad (x, y) \in D \tag{2.1c}$$

$$v(x, y, t) + U(x + t) = 0, \qquad (x, y) \in S, \quad t > 0, \tag{2.1d}$$

where v is outgoing at infinity. The quantities in (2.1) are dimensionless; the spatial variables have been scaled with respect to a characteristic length, L, of the target, the time with respect to L/c, where c is the speed of sound in D, and v and U with respect to the maximum of the incident pressure pulse.

Although we will use an explicit second-order finite-difference scheme to numerically approximate the solution of (2.1), we will initially keep our discussion general enough to cover other finite-difference schemes. Thus we consider a class of finite-difference methods for solving (2.1) that approximates the values of the scattered field at discrete points $(x_i, y_i) \in D$ for equally spaced discrete times. We write $v_i^{(m)}$ to denote the discrete approximation of the scattered field for the mth time step at the position (x_i, y_i). We denote grid points on the surface of the target by (X_p, Y_p) $(p = 1, ..., N)$. For numerical methods that respect the linearity, time invariance, and causality of the continuous problem (2.1), it can be shown (see Appendix A) that the response $v_i^{(m)}$ is exactly related to the incident wave as sampled by the grid points on the target by

$$v_i^{(m)} = \sum_{p=1}^{N} \left[\sum_{l=0}^{m} \mathscr{K}_{pi}^{(m-l)} U(X_p + lh) \right] \tag{2.2}$$

where h is the time step. The outer sum expresses the response at (x_i, y_i) as the superposition of the responses from the effect of the incident wave through the various grid points on the surface of the target; this is the discrete version of Huyghens principle. The inner sum expresses each of these contributions to the total response as a convolution of the incident wave (as sampled at the surface grid point) with a discrete transfer function. Alternatively, (2.2) can be interpreted as a discrete version of a Green's function representation of the scattered field where $\mathscr{K}_{pi}^{(m-l)}$ is the Green's function evaluated at the spatial points (X_p, Y_p), (x_i, y_i) and the shifted temporal point.

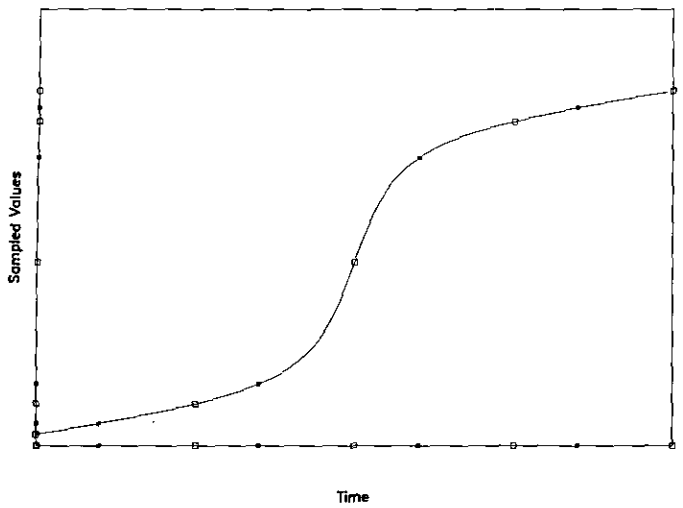

FIG. 2.1. Sampling on a staggered grid.

The Multi-source Problem

Equation (2.2) is an imperfect discrete analogue of (1.1). This imperfection is the critical issue in the development of a discrete formula for predicting the secondary scatter wave. The root of the difference between the continuous and discrete cases arises from the way the incident pulse is seen on the surface of the target. In the continuous case, the incident pulse seen at any two points on the surface of the target is exactly the same except for a possible time delay. In the discrete case, if the distance in the direction of travel of the incident wave between the two points on the surface is not a integral multiple of h then the discrete time series viewed at the two point generally differs by more than just a time delay as illustrated in Fig. 2.1, where the solid square denotes the incident field at a spatial grid point and the open square at the other. That is, because the delay is not a integral multiple of h, the two discrete time grids on which the incident wave is sampled are staggered, and the sampled discrete time series are potentially completely independent. The potential degree of independence is illustrated in Fig. 2.2, where the discrete time series sampled on the grid marked by solid squares is increasing while that sampled on the grid marked with outlined squared is decreasing. Thus, where in (1.1) we have the continuous response to a single continuous input, in (2.2) we have the discrete response to N independent inputs.

For $N > 1$ a single numerical experiment is insufficient to deduce how N independent inputs produce an output. Based on (2.2) the secondary pulse prediction problem has exactly this intractable structure. We call this difficulty the *multi-source problem.* Its resolution is based on the observation that we are generally interested in the situation where the time step h is chosen to adequately resolve the incident pulse (unlike in Fig. 2.2). In such cases, the observations on a grid can be inferred to a high degree of accuracy from those on a staggered grid through an interpolation formula. Our solution to the multi-source problem is to modify the incident pulse profiles so that the interpolation formula can be used exactly. Of the many modifications of this kind perhaps the simplest is to sample the continuous pulse profile on a reference grid with spacing h and to redefine the values of the pulse profile through linear interpolation as shown in Fig. 2.3.

To implement and analyze the interpolation formula, we make use of two functions. The first $M(x)$ is the smallest integer such that $x \leqslant hM(x)$; the second is defined by $H(x) = M(x) - x/h$. Thus, $M(x)$ gives the number of full h-sized steps needed to cover the interval $[0, x]$, and $H(x)$ gives the fraction of the last step that extends beyond x. We define the standard discrete sample $w_m = U(X_0 + mh)$. Assuming that (X_0, Y_0) is the first discrete point on the

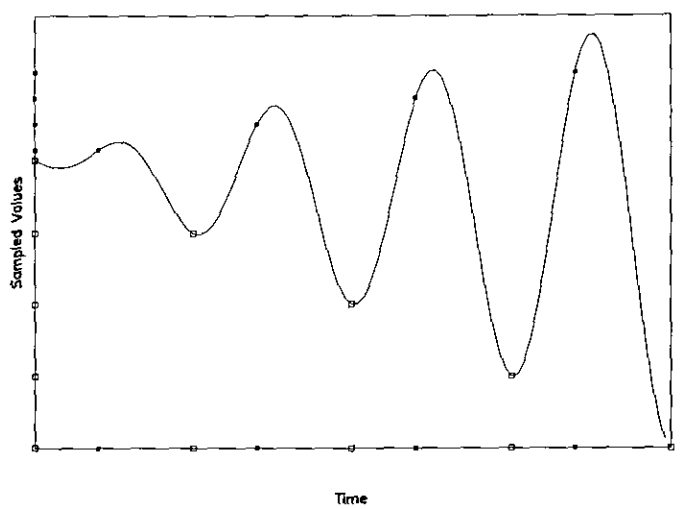

FIG. 2.2. Independence of the staggered samples.

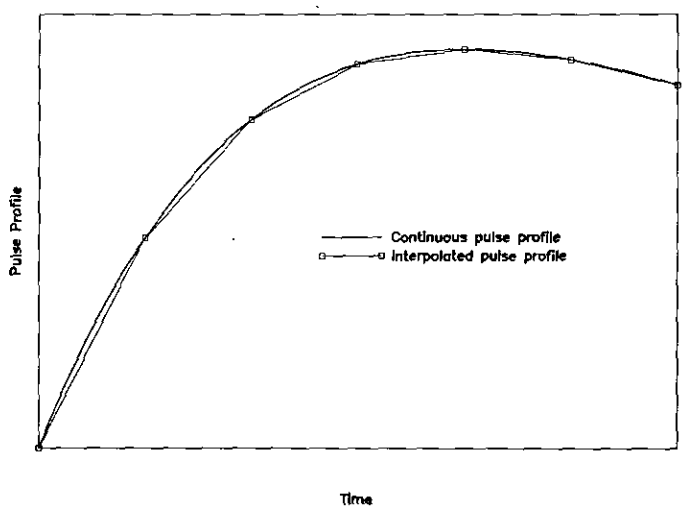

FIG. 2.3. Piecewise linear interpolation of a pulse profile.

target hit by the incident pulse, we see that $w_m = 0$ for $m < 0$. A modified continuous pulse profile $W(x)$ approximating $U(x)$ is constructed from w_m using the interpolation formula

$$W(X_0 + x) = \sum_{j=0}^{M(x)} a_j(H(x))\, w_{M(x)-j}. \tag{2.3}$$

In the case of piecewise linear interpolation $a_0(H) = 1 - H$, $a_1(H) = H$, and $a_l(H) = 0$ for $l \geqslant 2$.

Using (2.3) the modified incident pulse as sampled at (X_p, Y_p) at the lth time step is

$$W(X_p + lh) = \sum_{j=0}^{M(X_p - X_0 + lh)} a_j(H(X_p - X_0 + lh) \times w_{M(X_p - X_0 + lh) - j}. \tag{2.4a}$$

Because $M(X_p - X_0 + lh) = M(X_p - X_0) + l$ and $H(X_p - X_0 + lh) = H(X_p - X_0)$, we can rewrite (2.4a) as

$$W(X_p + lh) = \sum_{j=0}^{l} \alpha_{pj} w_{l-j}, \tag{2.4b}$$

where $\alpha_{pj} = a_{M(X_p - X_0)+j}(H(X_p - X_0))$ when $j + M(X_p - X_0) \geqslant 0$ and $\alpha_{pj} = 0$ when $j + M(X_p - X_0) < 0$. Approximating $U(x_p + lh)$ in (2.2) with $W(x_p + lh)$ as given by (2.4b) yields (after a considerable amount of algebra)

$$v_i^{(m)} = \sum_{j=0}^{m} \sum_{p=1}^{N} \sum_{l=0}^{m-j} \mathscr{K}_{pi}^{(m-j-l)} \alpha_{pl} w_j. \tag{2.5}$$

Letting

$$K_i^{(\mu)} = \sum_{p=1}^{N} \sum_{l=0}^{\mu} \mathscr{K}_{pi}^{\mu - l} \alpha_{pl}, \tag{2.6}$$

we can rewrite (2.5) in a form completely analogous to (1.1):

$$v_i^{(m)} = \sum_{j=0}^{m} K_i^{(m-j)} w_j.$$

This results shows that preconditioning the incident pulses using (2.3) converts (2.2) into (2.6) which overcomes the multi-source problem.

A Procedure for Predicting the Secondary Scattered Wave

The significance of (2.6) is that the kernel K_i^{μ} can be inferred from a single numerical experiment. Thus, the response $\tilde{v}_i^{(m)}$ to a secondary incident pulse profile with sampled values $\tilde{w}_j$ can be computed from (2.6) without directly performing a second numerical experiment. In principle, the kernel K_i^{μ} may be deduced from any nonzero incident pulse, but the required deconvolution process is in many cases unstable when performed in finite-precision arithmetic. Rather than consider the general case, we present a particular incident pulse for which deduction of the kernel from a numerical experiment is computationally trivial and completely stable.

The incident wave is the "Kronecker" pulse $U(x) = 1$ for $x = 0$ and 0 elsewhere, which neither represents a discrete approximation to the delta function nor any smooth function. Nonetheless when this pulse is preconditioned by the linear interpolation scheme corresponding to (2.3), it can be used as the input for a finite-difference code and the output $v_i^{(m)}$ can be unequivocally determined. Since the w_j corresponding to this pulse are given by $w_j = \delta_{0j}$, where δ_{ij} is the Kronecker delta function, it follows from (2.6) that the kernel is explicitly given by

$$K_i^{(\mu)} = v_i^{(\mu)}. \tag{2.7}$$

Our procedure for deducing the scattered field $\tilde{v}$ from a second incident pulse $\tilde{U}$ is now evident. The second pulse is sampled to obtain $\tilde{w}_m = \tilde{U}(X_0 + mh)$. Then, we insert these values and the values for the kernel obtained from (2.7) into (2.6) to obtain the explicit result

$$\tilde{v}_i^{(m)} = \sum_{j=0}^{m} v_i^{(m-j)} \tilde{w}_j. \tag{2.8}$$

Several factors affect the usefulness of (2.8) for a given application. The most significant is that (2.8) gives the response of the interpolated pulse profile $\tilde{W}$ rather than that of the original pulse profile $\tilde{U}$. When the interpolated pulse is a poor approximation of the actual pulse (i.e., the interpolation is too coarse), the prediction of (2.8) is unlikely to be satisfactory. This limitation, however, is unlikely to cause practical difficulties because the failure of the interpolated pulse to approximate the actual pulse indicates that the actual pulse is not adequately resolved on the given grid and that the numerical method is unlikely to give meaningful results.

Another factor affecting the choice between using (2.8) or repreating the numerical experiment is the relative numerical efficiency of the methods. In a direct implementation of (2.8), computation of the response value $\tilde{v}_i^{(\mu)}$ for $\mu = 1, \ldots, m$ requires $O(m^2)$ operations while repeating the numerical experiment requires $O(Pm)$ operations, where P is the number of discrete point in the computational domain. Since P is typically large, even the $O(m^2)$ implementation of (2.8) may be advantageous. Using the fast Fourier transform to perform the convolution in (2.8) reduces the operation count for the prediction procedure to $O(m \log m)$ which makes this procedure very competitive, especially when the numerical experiment is based on a method that requires a

large amount of computation for a single step as is often the case for implicit schemes.

The prediction procedure also has the particular advantage that when the response at a small number of points in space and time are needed, the computation of the response at other points is not a necessary intermediate step. For example, obtaining the long-time harmonic response in the near field requires no computation of values for short times or in the far field. These advantages of the prediction procedure suggests that it should find many applications.

Finally, we observe that the finite-difference method and the associated discrete radiation boundary condition (see Section III) produce errors in the v_l^μ. The former produces numerical dispersion which is sensative to the high-frequency content of the Kronecker function while the latter is sensitive to its low-frequency content. (Here the frequency content is measured with respect to the size of the grid.) The same errors would also be present in a direct finite-difference simulation of a scattering problem for a smooth incident pulse. Thus, our method is only as good as the underlying difference scheme and its associated radiation boundary condition in resolving both the high-frequency and low-frequency contents of a given incident pulse. If one knew a priori the class of incident pulses that were to be used in scattering experiments, then a mesh size and the position of the radiation boundary condition could be determined to ensure that our method produced accurate results.

III. NUMERICAL EXPERIMENTS

In this section, numerical experiments that illustrate and confirm the theoretical results of earlier sections are presented. A numerical simulation of the problem given in (2.1) for a sound-soft circular cylinder is conducted for a collection of incident pulse profiles. The performance of the prediction procedure (2.8) is evaluated for each of these experiments. No error in the predicted scattered waves is detected in these experiments up to seven significant figures. Similar results for a Helmholtz-like resonator indicate the applicability of our method is not restricted to simple scatterers.

The Numerical Method

We use a finite-difference scheme to approximate solutions of (2.1). The surface of the target S is a circle with radius one. The scheme implemented is the standard explicit centered-difference scheme in polar coordinates which is mildly dispersive. Furthermore, we make use of an artificial nonreflecting boundary at a radius R from the center of the circular target. This boundary [6] is nonreflecting only to first order and produces an error of $O(1/R^2)$. The finite-difference scheme is second-order accurate. That the approximate solutions of (2.1) bear some marks of the deficiencies of the numerical method is of little concern to us as we are interested in the prediction of one numerical experiment from another, not in the quality of the experiments. In fact, the ability of the prediction procedure to resolve these numerical artifacts is an additional demonstration of its power.

Unless otherwise noted the numerical experiments use a target radius of 1, an artificial nonreflecting boundary at a radius of $R = 20$, 190 grid points in the radial direction, 32 grid points in the angular direction, a time step of 0.02, and a total of 2500 time steps. The computations are performed using double-precision arithmetic in a C language program. The results of the numerical scattering experiments are recorded in decimal format with 16 significant figures.

The output recorded in the experiment was not the field values $v_l^{(m)}$ but rather a numerical approximation of the normal derivative of the field values on the surface of the target. In principle, this information is sufficient to reconstruct the output field values. Because the normal derivative is linearly related to the field values the prediction formula (2.7) still applies. Thus, in this section $v_l^{(m)}$ denotes the normal derivative of the field on the surface of the target because this quantity plays the same role (the output of the numerical experiment) as the field values did in the earlier sections.

The Incident Pulses

The incident pulse profiles in the tests are the Kronecker function, two unmodulated gaussian profiles, two stepped-sine profiles, and two modulated gaussian profiles. A designation, a description, and an explicit formula for the sampled values are given for each pulse profile in Table I.

Figure 3.1 presents plots of the various incident pulse profiles. We note that the maximum value of the amplitude for each pulse is one.

The Response to a Kronecker Function

We first examine the response to the Kronecker function. We examine this response and the responses to most of the

TABLE I

Pulse Profiles for the Numerical Experiments

Designation	Description	Formula
(K1)	Kronecker function	$w_0 = 1,\ w_l = 0\ (l \geq 1)$
(G1)	Fat guassian	$w_l = \exp(-(l/50-4)^2)$
(G2)	Thin gaussian	$w_l = \exp(-(l/25-4)^2)$
(S1)	Slow stepped-sine	$w_l = \sin(l/50)$
(S2)	Fast stepped-sine	$w_l = \sin(3\pi l/50)$
(M1)	Slow modulated gaussian	$w_l = \exp(-(l/50-4)^2)\sin(l/10)$
(M2)	Fast modulated gaussian	$w_l = \exp(-(l/50-4)^2)\sin(l/50)$

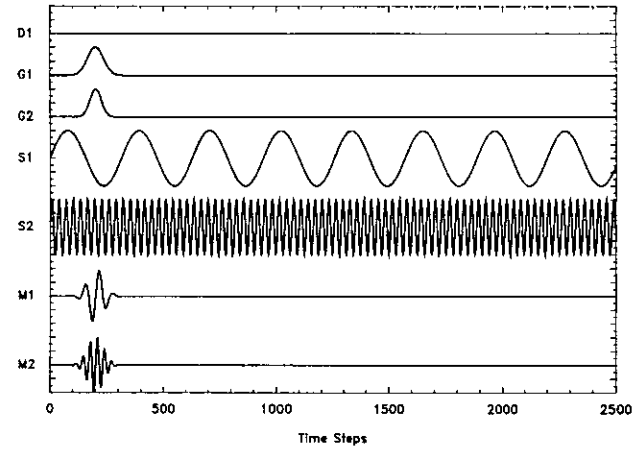

FIG. 3.1. Incident pulse profiles for numerical experiments.

other pulses only at the front of the target. Nonetheless, the observations we make reguarding this response apply uniformly to all points around the target. There is no discernible degradation of the predicon method at the rear of the target. Except to illustrate this point, we limit discussion to the front of the target only to make the presentation as concise as possible.

The response to a preconditioned Kronecker function computed using the numerical method described above is shown in Fig. 3.2a and 3.2b. Elements of this response are unphysical in the sense that the Kronecker function strongly excites frequencies not well resolved on the grid. Grid refinement does not suppress these features because the duration of the Kronecker pulse is defined to be one time step. The CFL condition limits refinement of the spatial grid. Thus, the calculated response to a Kronecker pulse is expected to contain numerical artifacts due to grid dispersion and imperfections in the nonreflecting boundary conditions. Nonetheless, these numerical artifacts are of little concern because we do not use the response to the Kronecker function as a model of the physical response to a delta function. Rather our goal is to use the response to a Kronecker function as an intermediate step in predicting the numerical response to other pulses. Because grid dispersion affects higher frequencies most strongly, most numerical artifacts are removed when the response to the Kronecker function is convolved with a incident pulse profile whose spectral content is mostly in the low-frequency range.

Predicting the Response to a Secondary Incident Profile

The chief result of the numerical tests is that no difference between the predictions and the finite-difference-based numerical experiments is evident to seven significant figures. Thus, the predicted and usual responses shown in the figures of this section are in fact the same curve. This essentially perfect prediction holds uniformly at the various grid points around the target.

Figures 3.3 and 3.4 show the response to the two gaussian pulses (G1) and (G2).. There is no discernible difference between the numerically computed response and that predicted from the response to the Kronecker function. Indeed, even the small reflection from the artifical boundary at $R = 20$ is accurately predicted. Thus, our method can extract the physically meaningful low-frequence response of the system at long times in spite of numerical artifacts of the underlying numerical method.

Figures 3.5 and 3.6 show the response to the two stepped-sine pulses (S1) and (S2). Again the prediction of the numerical experiment is perfect. Thus, the prediction procedure can predict the harmonic response for a broad range of frequencies from a single numerical experiment, as well as the underlying numerical method allows. The ability to predict the long-term behavior after the transients decay is of particular interest.

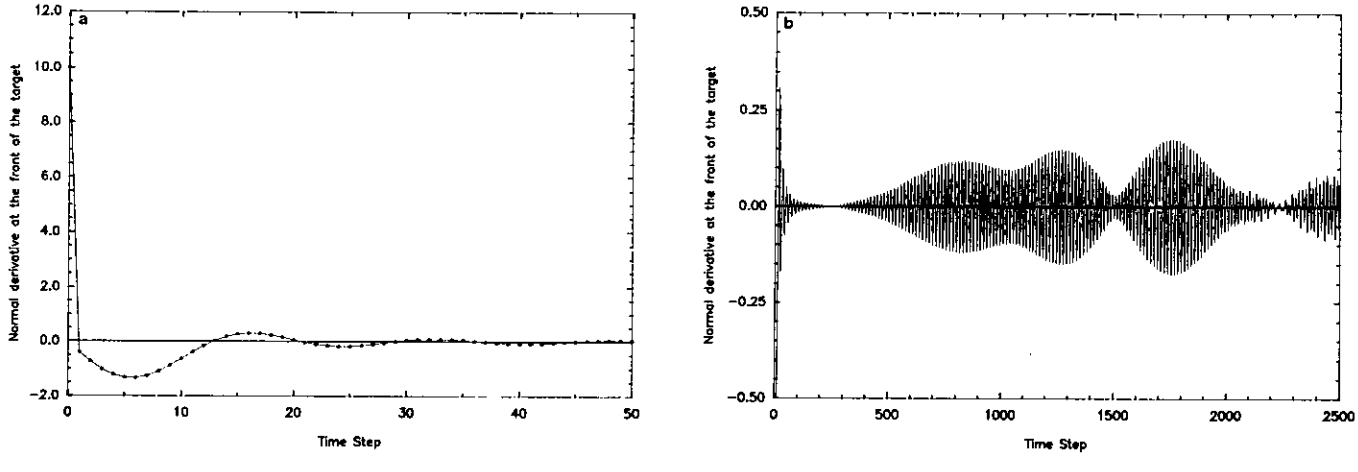

FIG. 3.2. Response to the Kronecker function (K1): (a) short-time; (b) long-time.

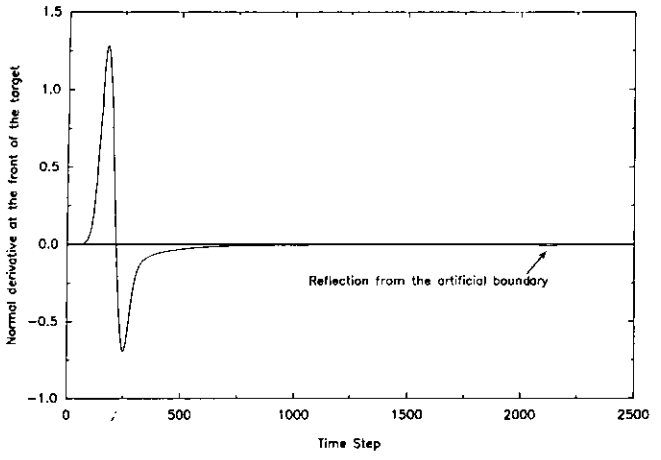

FIG. 3.3. Predicted and actual response for G1.

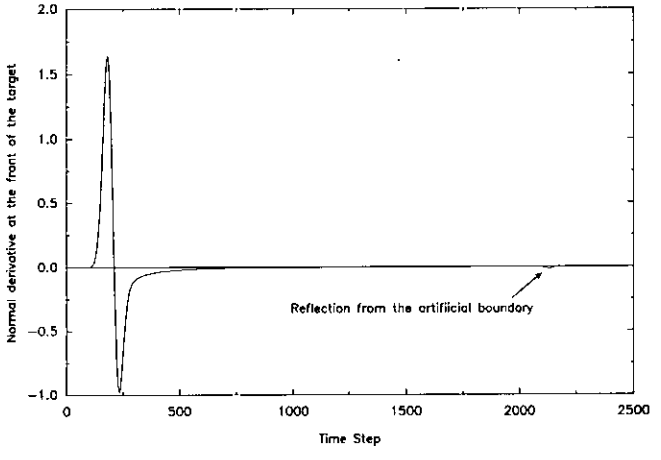

FIG. 3.4. Predicted and actual response for G2.

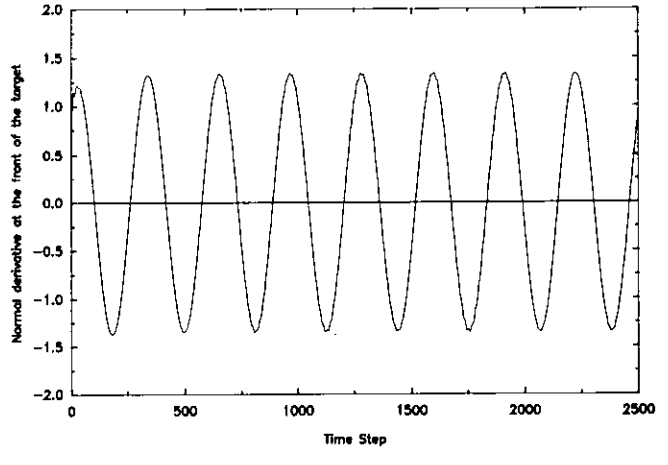

FIG. 3.5. Predicted and actual response for S1.

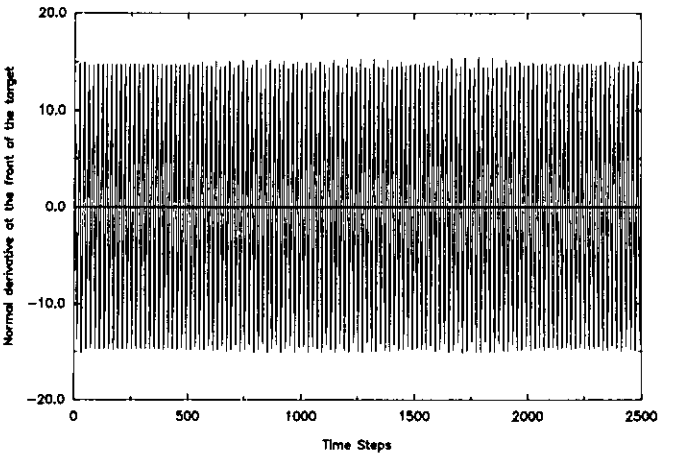

FIG. 3.6. Predicted and actual response for S2.

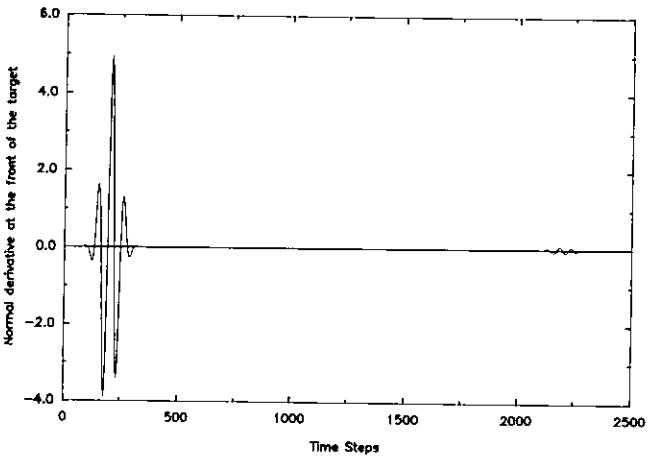

FIG. 3.7. Predicted and actual response to M1.

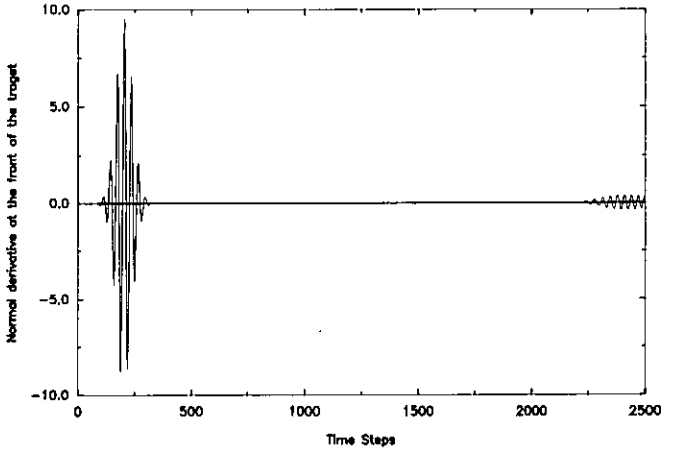

FIG. 3.8. Predicted and actual response for M2.

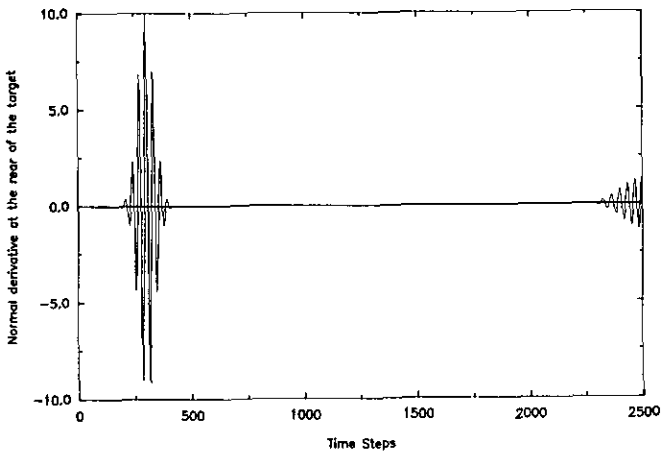

FIG. 3.9. Predicted and actual response in the shadow for M2.

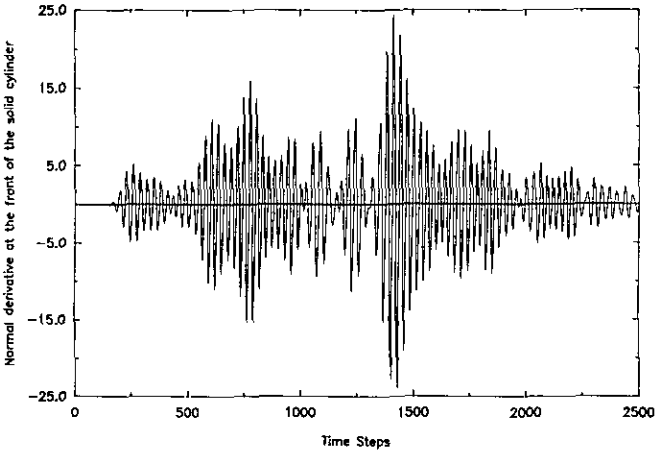

FIG. 3.10. Response of a Helmholtz-like resonator for M2.

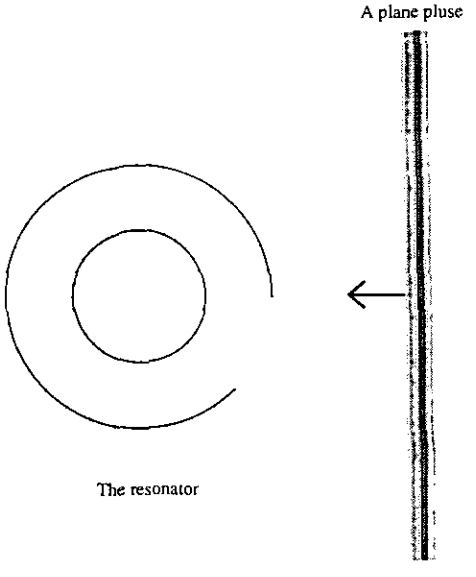

FIG. 3.11. A Helmholtz-like resonator.

Figures 3.7 and 3.8 show the response to the modulated gaussian pulses (M1) and (M2). The modulated gaussian pulses are perhaps the most sever test of the prediction method because they contain two widely separated scales (the period of the modulating sine function and the width of the gaussian envelope). Nonetheless, the prediction method performs without error to seven significant figures including resolving the reflection from the artificial boundary.

Figure 3.9 shows the response to (M2) at the rear of the target. In the shadow region the prediction method is still essentially perfect. This result says that the prediction method anticipates the results of a numerical experiment perfectly. It does not imply that quality of the numerical experiment is the same at the front and rear of the target.

Figure 3.10 shows the response to (M2) at the front of a Helmholtz-like resonator. Again no difference between the prediction and the numerical response is found. This resonator consists of the cylinder used in the earlier experiments surrounded by a slit-cylinder of radius two (see Fig. 3.11). The slit spans an arc of 45° beginning at the front of the target. This asymmetric resonator produces a response considerably more prolonged and complicated than that for a simple cylinder. The quality of the prediction suggests the general applicability of the method to complicated scatterers, including those consisting of inhomogeneous penetrable materials.

IV. CONCLUSIONS

We have presented a new method which approximately determines the scattering of a scalar wave off an impenetrable target and have given numerical examples for a sound-soft object. The method is a discrete analog of a familiar convolution result for linear systems in which the kernel contains all the physical information about the scatterer. We deduce an algorithm for approximating this kernel and we determine an explicit solution to it by running a single scattering experiment. Specifically, we use an explicit finite-difference scheme (other methods can also be used) to determine the discrete field produced by an incident Kronecker pulse and this field is used to determine an approximate kernel. To determine a numerical approximation of the scattered field for a given incident pulse we simply apply our discrete convolution formula using the incident pulse and the approximate kernel.

We observe that our method faithfully produces the same errors in the scattered fields as would a direct application of the explicit finite-difference scheme. The errors introduced by using the finite-difference scheme to compute the response of the incident Kronecker pulse seem to propagate their way through the convolution formula to do this. These errors come about from the discretization of the underlying equations and boundary conditions, and the application of a radiation boundary condition at a finite radius. They can

be reduced by more refined spatial discretization and by either larger computational domains or higher order boundary operators, respectively. The former would require prohibitively small temporal steps for the explicit method used in this paper. If very low errors are required from a numerical simulation, then the above arguments suggests that an implicit scheme would be used to solve the scattering problem with the incident Kronecker pulse. Our method would then produce a truly economical means by which to accurately solve other scattering problems.

Finally, we observe that our method can be extended in principle to solve scattering problems from penetrable targets. That is, scatterers whose physical properties are inhomogeneous. This extension is the subject of ongoing research activities.

APPENDIX A

In this appendix we derive (2.2) which characterizes the class of linear, time invariant, causal numerical methods for solving (2.1) considered in Section II and III. According to (2.1d) the scattered waved v is driven by the values of the incident profile on the surface of the target. Thus, we expect that the numerical estimate of the scattered wave $v_i^{(m)}$ is a linear function of the discretely sampled incident waves $U(X_p + mh)$. The most general linear function of this kind has the form

$$v_i^{(m)} = \sum_{p=1}^{N} \sum_{l=-\infty}^{\infty} \beta_{impl} U(X_p + lh). \tag{A1}$$

That is, the linear function is completely characterized by the constants β_{impl}.

That the numerical method is time invariant means that if the incident waves is delayed (shifted in time) by L time steps then the response is also delayed by L steps. Thus,

$$v_i^{(m-L)} = \sum_{p=1}^{N} \sum_{l=-\infty}^{\infty} \beta_{impl} U(X_p + lh - Lh). \tag{A2a}$$

Shifting the dummy index l and the discrete time m, (A2a) may be rewritten as

$$v_i^{(m)} = \sum_{p=1}^{N} \sum_{l=-\infty}^{\infty} \beta_{im+Lpl+L} U(X_p + lh). \tag{A2b}$$

which implies that

$$\beta_{im+Lp+L} = \beta_{impl} \tag{A3}$$

for all values L. This result says that β_{impl} depends on l and m only through their difference $m-l$. That is, there exist constants $K_{pi}^{(\mu)}$ such that $\beta_{impl} = K_{pi}^{(m-l)}$. Substituting this result into (A1) yields

$$v_i^{(m)} = \sum_{p=1}^{N} \sum_{l=-\infty}^{\infty} K_{pi}^{(m-l)} U(X_p + mh). \tag{A4}$$

Causality requires that $v_i^{(m)}$ depends only on the nonzero portion of the incident wave reaching the target up to the mth time step. Thus, the inner sum in (A4) can be restricted to run from $l=0$ to $l=m$, giving (2.2).

REFERENCES

1. S. I. Hariharan, U. Ping, and J. R. Scott, *J. Comput. Phys.* **101**, 419 (1992).
2. D. Givoli, *Numerical Methods for Problems in Infinite Domains* (Elsevier, Amsterdam, 1992), Chap. 11.
3. G. A. Kriegsmann, *Wave Motion* **4**, 371 (1982).
4. S. I. Hariharan, J. S. Wong, and N. Ida, *Review of Progress in Quantitative Nondestructive Evaluation*, edited by D. Thompson and D. Chimenti (Plenum, New York, 1989), p. 259.
5. N. K. Madsen and R. W. Ziolkowski, *Wave Motion* **10**, 583 (1988).
6. A. Bayliss and E. Turkel, *Commun. Pure Appl. Math.* **33**, 707 (1980).